Rossby wave analysis of the baroclinic potential energy in the upper 500 meters of the North Pacific

by James M. Price[1] and Lorenz Magaard[1]

ABSTRACT

Time series of baroclinic potential energy in the upper 500 meters of the North Pacific (20-50N, 145E-130W) prepared by White (1977a) are analyzed by spectral and cross-spectral methods in the period range from 2 to 10 years.

Maximum energy occurs in the 7 to 10 year range over the entire data field. In the 20-30N zone we find first order baroclinic Rossby waves with wave lengths of about 1000 to 3000 km to be the dominating phenomenon in the 7 to 10 year range. In this zone they occur also in the 2 to 7 year range but to a much lesser extent. North of 30N, however, baroclinic Rossby waves play no role in the entire 2 to 10 year range.

In parts of the eastern half of the 20-30N zone the Rossby waves show a consistent refraction pattern hinting at possible coastal generation of these waves.

1. Introduction

Emery and Magaard (1976), henceforth referred to as EM, showed that a random field of first mode baroclinic Rossby waves could account for 60 to 80 percent of the variance of the observed subsurface temperature structure between Hawaii and weather station November (30N, 140W). This was done with a cross-spectral fit of a wave model to the observed temperature fluctuations. In a follow-up study Magaard and Price (1977), henceforth referred to as MP, generalized EM's wave model to incorporate all possible wave number vectors, not just those conforming to the baroclinic Rossby wave dispersion relation at a given frequency. They found that in all cases the best fit was obtained at frequency-wave number combinations conforming to Rossby waves.

Motivated by these results, we obtained the data set used by White (1977a) in his study of the variability of the baroclinic structure of the interior of the North Pacific. This data set encompasses a much greater area than that studied by EM, thereby offering the opportunity to study the occurrence and possible refraction of Rossby waves in an extended area, as well as possible effects of current shear and bottom topography on such a wave field.

1. Department of Oceanography, University of Hawaii, Honolulu, Hawaii, 96822, U.S.A.

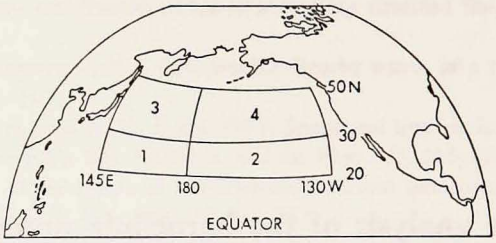

Figure 1. Area of data coverage. Four subareas are indicated.

2. The data

The data set used in this study is based upon the National Oceanographic Data Center's hydrographic file for the North Pacific. Observations over the region 20-50N, 145E-130W (Fig. 1) during the years 1950-1970 and extending below 500 meters depth were compiled and processed by White (1977a) into the residual baroclinic potential energy time series, RBPE, used herein. The RBPE values exist on a 5-degree latitude by 5-degree longitude by one-year grid.

Two possible problems should now be considered. First, the RBPE is a vertically integrated quantity, thus a study of the vertical mode structure is not possible. Based upon the findings of EM, we restrict this study to a hypothetical first mode wave. In addition, the vertical integration contaminates the data with other processes manifest in the surface layer, however, a substantial portion of the RBPE fluctuations may still be accountable by Rossby waves.

Second, at many locations in the data field there are fewer than five years coverage of hydrocast data, and for many years between 1950 and 1970 fewer than 50 percent of the 5-degree subdivisions contained hydrocast data, White (1977a). Thus, even with the optimum interpolation, some doubt may be raised about the suitability of this data set for such a wave study. However, Rossby waves with periods of years and wave lengths of thousands of kilometers may be manifest in this data set despite the gaps.

We divide the data field into four smaller subareas (Fig. 1). The criteria employed in choosing the boundaries were topography and the North Pacific Current. West of 180 the bottom topography is considerably rougher than east of 180, and 30N may be taken as the southernmost extent of the North Pacific Current. Thus, these four subareas are physically different regimes, and it is interesting to view the findings of this study with that in mind.

3. Features of the energy spectra

As a preliminary survey of this data set, we examine the energy spectra of the RBPE time sequences at each grid point. A spectral peak at the 10-year period, significant at the 80% confidence level, was frequently found, followed by a roughly

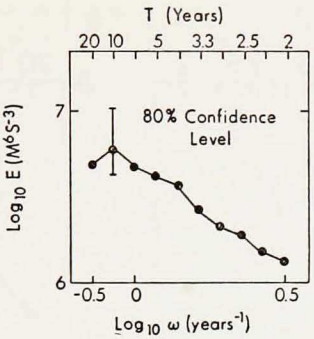

Figure 2. Composite spectrum from the entire data field. E is the energy per unit frequency.

monotonic decrease in energy at the lower periods. The composite spectrum computed by averaging the individual spectra computed at all the grid points (Fig. 2) shows these features. The composite spectrum for each of the subareas (Fig. 4) predominantly shows these same features. However, in subareas 1 and 2, spectral energy increases at the lower periods, and, in subarea 1, a "plateau" at the higher periods exists instead of a spectral peak. This "plateau" shows significantly higher energy (at the 80% level) at the 4 year period and almost significantly higher energy at the 5 and 3.3 year periods than would be expected if the energy decreased linearly with decreasing period. The higher spectral energies at all periods in the western subareas are in accord with the greater RBPE variance found by White (1977a) in the Western Pacific. And finally, Figure 3 shows composite spectra derived from combinations of two subareas. In these spectra, peak energy is again found at the 10 and 6.7 year periods. Larger spectral energy is found in the west, and the lower latitude spectra exhibit an increase in energy at the lower periods.

Further information about the geographic distribution of spectral energy within the RBPE field is displayed in Figure 5. This figure maps the periods corresponding to high spectral energy (not necessarily spectral peaks) found at each grid point. Careful examination shows that 20-, 10-, 6.7-, and 4-year periods occur ubiquitously as high energy contributions to the spectrum, but the 10 and 6.7 year periods seem more numerous east of 180. The 5- and 3.3-year periods occur less frequently as high-energy contributors and also are found more frequently east of 180. The lower periods, 2.9, 2.5, and 2.2 years, appear sparsely in subarea 1, where, despite the previously mentioned trend toward increasing energy at the lower periods, the higher periods dominate.

As a final step in our preliminary analysis, we compute the maximum entropy spectra (using the Burg algorithm) of the RBPE sequences and compare them to the corresponding "conventional" spectra at several grid points. Since these RBPE sequences contain only 20 points, a comparatively short record, it seems plausible that this higher resolution spectral method might reveal more structure. However,

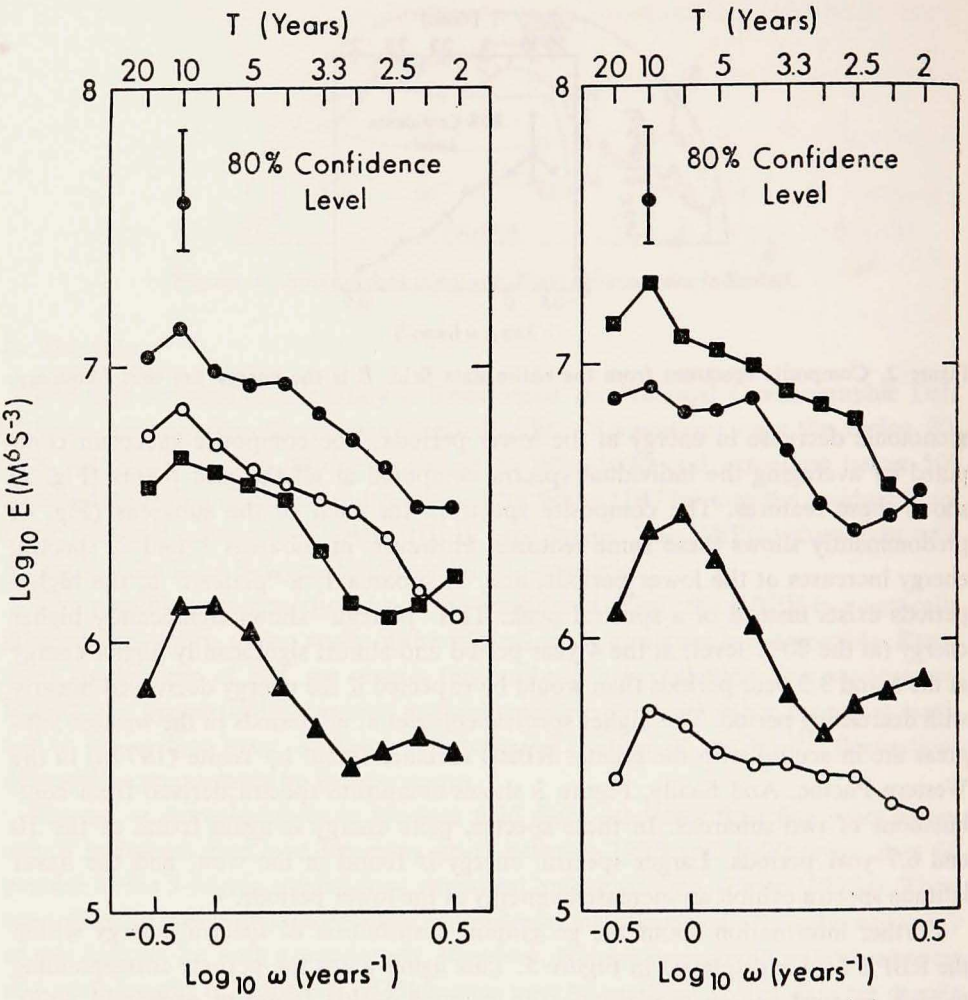

Figure 3. Composite spectra from subareas 1 and 3 (●), 2 and 4 (▲), 1 and 2 (■), 3 and 4 (○).

Figure 4. Composite spectra from subarea 1 (●), 2 (▲), 3 (■), 4 (○).

this is not the case; the two methods yield qualitatively similar spectra. (No error bars are computed for the maximum entropy spectra.) Four representative examples are given in Figure 6.

4. Method of Rossby wave analysis

Essentially, the wave model used in this study is the same as that used by EM and extended by MP, and the following text uses the same notation. In this analysis there is no vertical mode structure. $\phi_n(Z)$ in (5.1) of EM is set equal to one, and

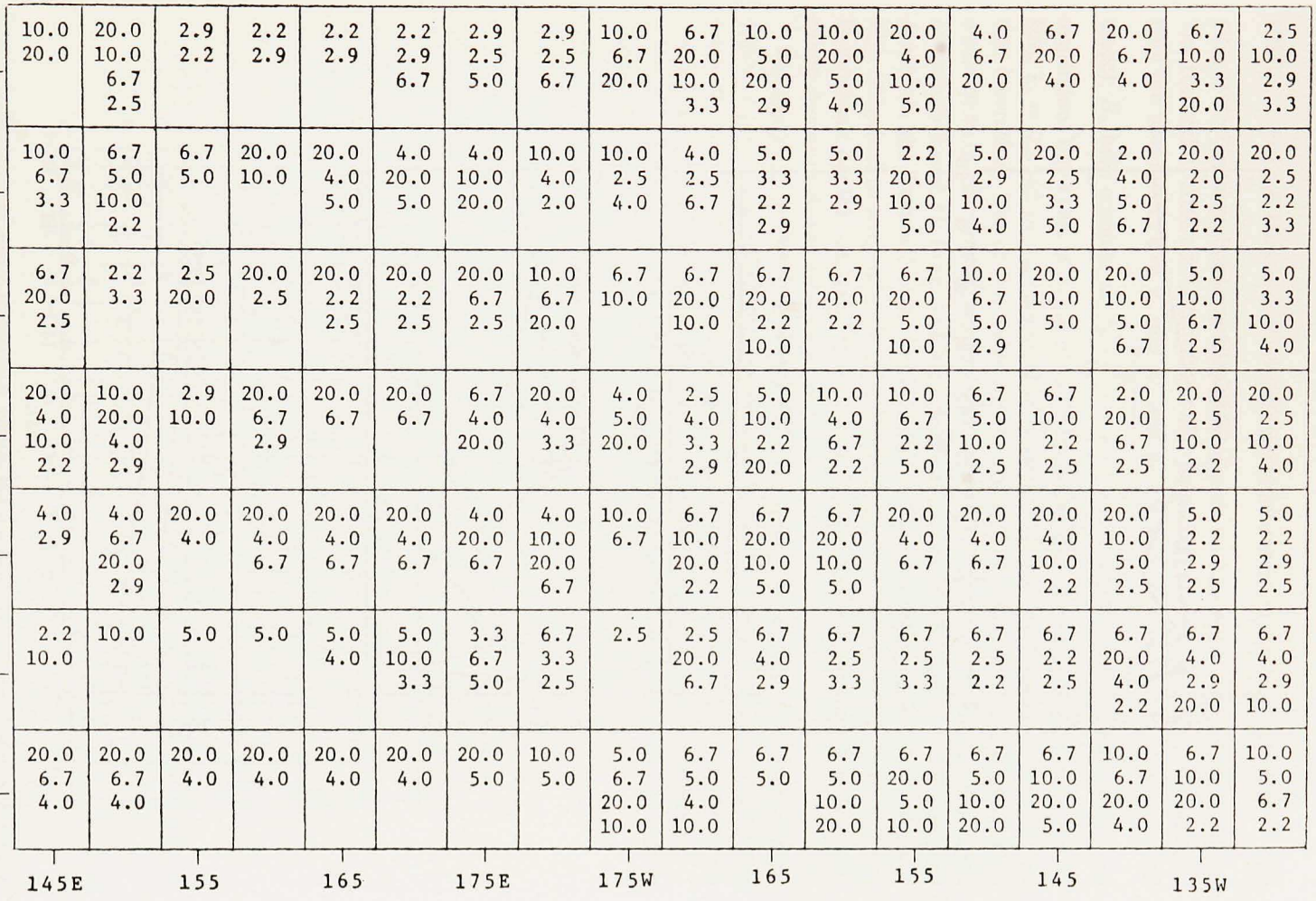

	145E		155		165		175E		175W		165		155		145		135W	
50N	10.0 20.0	20.0 10.0 6.7 2.5	2.9 2.2	2.2 2.9	2.2 2.9	2.2 2.9 6.7	2.9 2.5 5.0	2.9 2.5 6.7	10.0 6.7 20.0	6.7 20.0 10.0 3.3	10.0 5.0 20.0 2.9	10.0 20.0 5.0 4.0	20.0 4.0 10.0 5.0	4.0 6.7 20.0	6.7 20.0 4.0	20.0 6.7 4.0	6.7 10.0 3.3 20.0	2.5 10.0 2.9 3.3
45	10.0 6.7 3.3	6.7 5.0 10.0 2.2	6.7 5.0	20.0 10.0	20.0 4.0 5.0	4.0 20.0 5.0	4.0 10.0 20.0	10.0 4.0 2.0	10.0 2.5 4.0	4.0 2.5 6.7	5.0 3.3 2.2 2.9	5.0 3.3 2.9	2.2 20.0 10.0 5.0	5.0 2.9 10.0 4.0	20.0 2.5 3.3 5.0	2.0 4.0 5.0 6.7	20.0 2.0 2.5 2.2	20.0 2.5 2.2 3.3
40	6.7 20.0 2.5	2.2 3.3	2.5 20.0	20.0 2.5	20.0 2.2 2.5	20.0 2.2 2.5	20.0 6.7 2.5	10.0 6.7 20.0	6.7 10.0	6.7 20.0 10.0	6.7 20.0 2.2 10.0	6.7 20.0 2.2	6.7 20.0 5.0 10.0	10.0 6.7 5.0 2.9	20.0 10.0 5.0	20.0 10.0 5.0 6.7	5.0 10.0 6.7 2.5	5.0 3.3 10.0 4.0
35	20.0 4.0 10.0 2.2	10.0 20.0 4.0 2.9	2.9 10.0	20.0 6.7 2.9	20.0 6.7	20.0 6.7	6.7 4.0 20.0	20.0 4.0 3.3	4.0 5.0 20.0	2.5 4.0 3.3 2.9	5.0 10.0 2.2 20.0	10.0 4.0 6.7 2.2	10.0 6.7 2.2 5.0	6.7 5.0 10.0 2.5	6.7 10.0 2.2 2.5	2.0 20.0 6.7 2.5	20.0 2.5 10.0 2.2	20.0 2.5 10.0 4.0
30	4.0 2.9	4.0 6.7 20.0 2.9	20.0 4.0	20.0 4.0 6.7	20.0 4.0 6.7	20.0 4.0 6.7	4.0 20.0 6.7	4.0 10.0 20.0 6.7	10.0 6.7	6.7 10.0 20.0 2.2	6.7 20.0 10.0 5.0	6.7 20.0 10.0 5.0	20.0 4.0 6.7	20.0 4.0 6.7	20.0 4.0 10.0 2.2	20.0 10.0 5.0 2.5	5.0 2.2 2.9 2.5	5.0 2.2 2.9 2.5
25	2.2 10.0	10.0	5.0	5.0	5.0 4.0	5.0 10.0 3.3	3.3 6.7 5.0	6.7 3.3 2.5	2.5	2.5 20.0 6.7	6.7 4.0 2.9	6.7 2.5 3.3	6.7 2.5 3.3	6.7 2.5 2.2	6.7 2.2 2.5	6.7 20.0 4.0 2.2	6.7 4.0 2.9 20.0	6.7 4.0 2.9 10.0
20	20.0 6.7 4.0	20.0 6.7 4.0	20.0 4.0	20.0 4.0	20.0 4.0	20.0 4.0	20.0 5.0	10.0 5.0	5.0 6.7 20.0 10.0	6.7 5.0 4.0 10.0	6.7 5.0	6.7 5.0 10.0 20.0	6.7 20.0 5.0 10.0	6.7 5.0 10.0 20.0	6.7 10.0 20.0 5.0	10.0 6.7 20.0 4.0	6.7 10.0 20.0 2.2	10.0 5.0 6.7 2.2

Figure 5. Spectral periods corresponding to high energy in the spectrum computed at each grid point. The period corresponding to highest energy is listed at the top with lower energy periods following in order of decreasing energy.

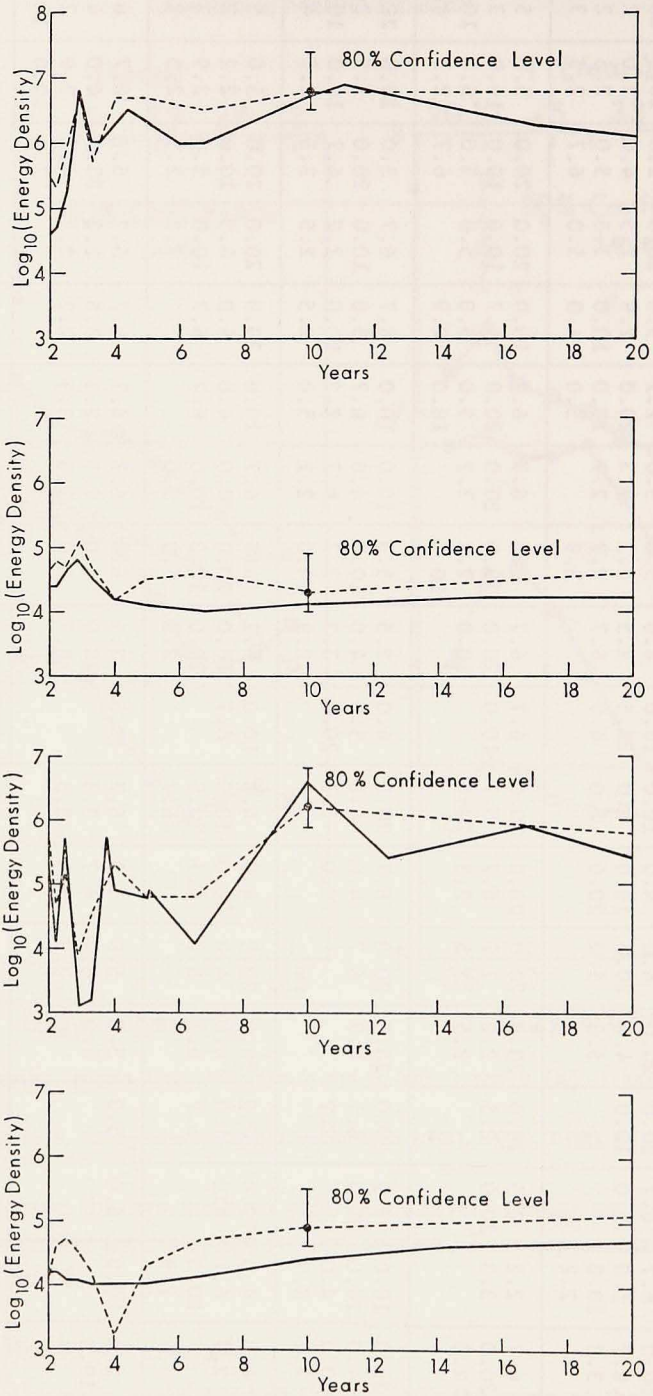

Figure 6. Comparison of maximum entropy spectra (solid curves) with corresponding conventional spectra (dashed curves) at 35N, 155E (a) 50N, 155E (b), 50N, 145E (c), and 50N, 150E (d).

ξ (in M^3S^{-2}) now represents a (two-dimensional) random field of RBPE fluctuations. The theoretical cross spectrum is now only a function of r and ω. Again, we consider only the first mode, $n = 1$, and R_1 and ϕ_1 are free parameters in the generalized model; R_1 held constant at $\sqrt{\frac{\beta^2}{4\omega^2} - f^2\lambda_1^2}$ constrains the model to Rossby wave dispersion. The value of λ_1 ((4.6) of EM) used in the latter case is the same used by EM, $\lambda_1 = 0.3343\ m^{-1}s$, computed from deep hydrocast data taken at weather station November. Use of this value for the entirety of subareas 1 and 2, the region where (4.6) of EM applies, seems reasonable when considering the nearly horizontal isopycnals found by Price and Meyers (1978) in zonal sections of mean potential density in the Central North Pacific. Mean N^2 profiles appear to vary much more with latitude than longitude. (A threefold increase in λ_1 decreases R_1 by an amount insignificant for this analysis for a 10 year wave; a twofold increase in λ_1 insignificantly decreases R_1 for a 2.2 year wave.)

We apply our model to four grid points at a time, namely to the corners of a 5-degree square. We systematically choose overlapping 5-degree squares until the entire data field is exhausted for the generalized model and, similarly, until subareas 1 and 2 data are exhausted for the model constrained to Rossby wave dispersion.

Error bars are computed for all fitting parameters by the same method used by EM and MP.

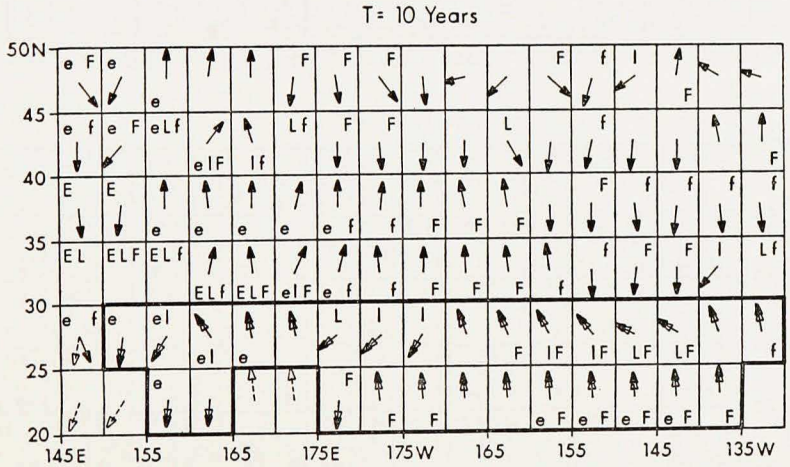

Figure 7. Direction of phase propagation determined by the generalized model (solid arrows) and by the Rossby wave model (open arrows) for wave period 10 years (a), 6.7 years (b), 5 years (c), 4 years (d), 3.3 years (e), 2.9 years (f), 2.5 years (g), and 2.2 years (h).

T = 6.7 Years

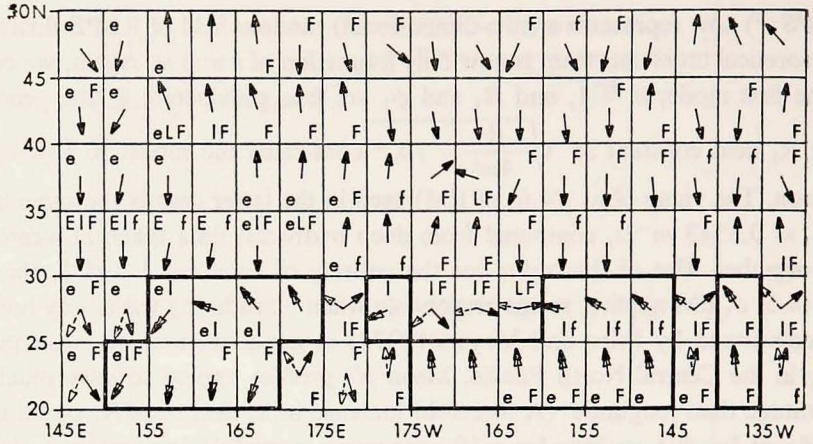

T = 5 Years

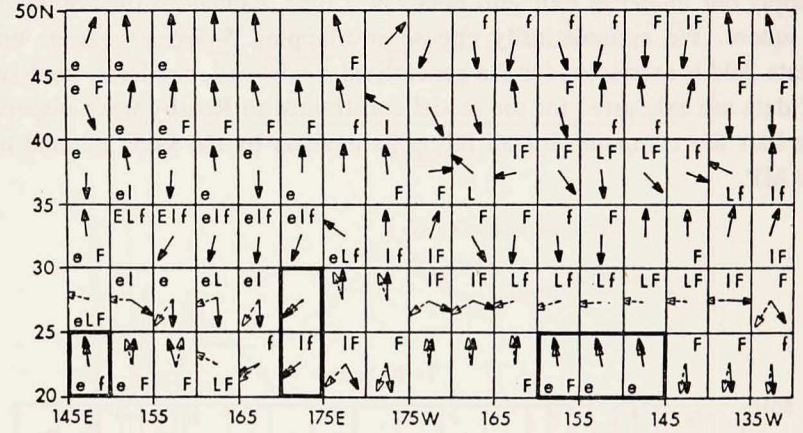

T = 4 Years

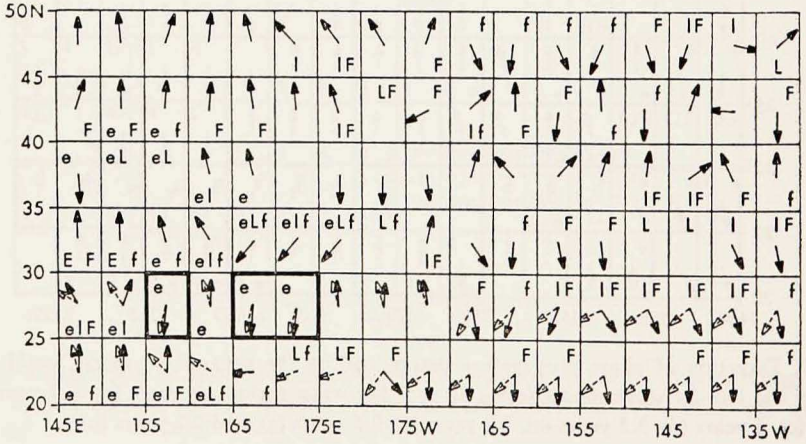

T = 33 Years

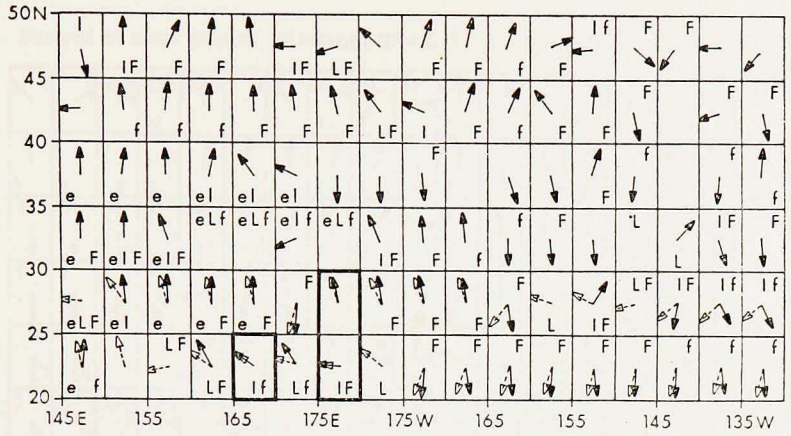

T = 2.9 Years

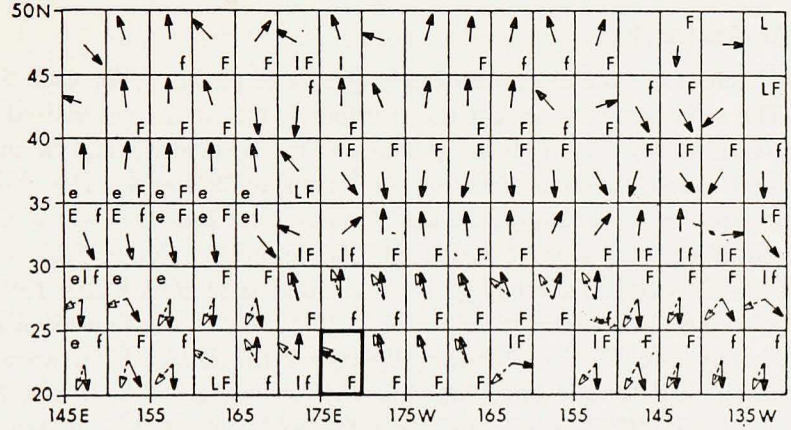

T = 2.5 Years

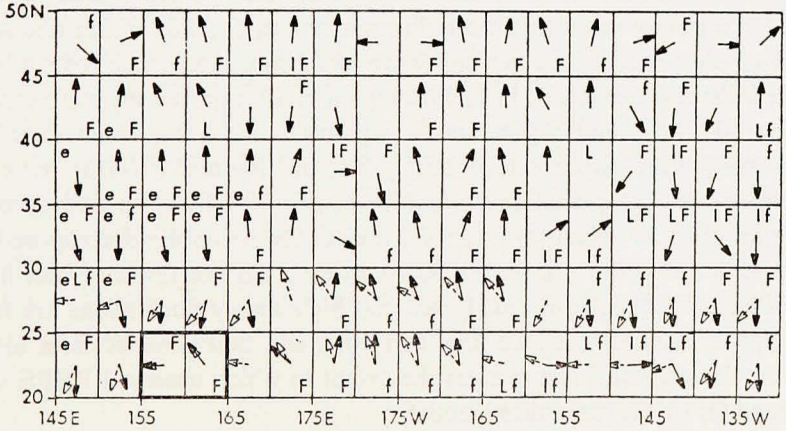

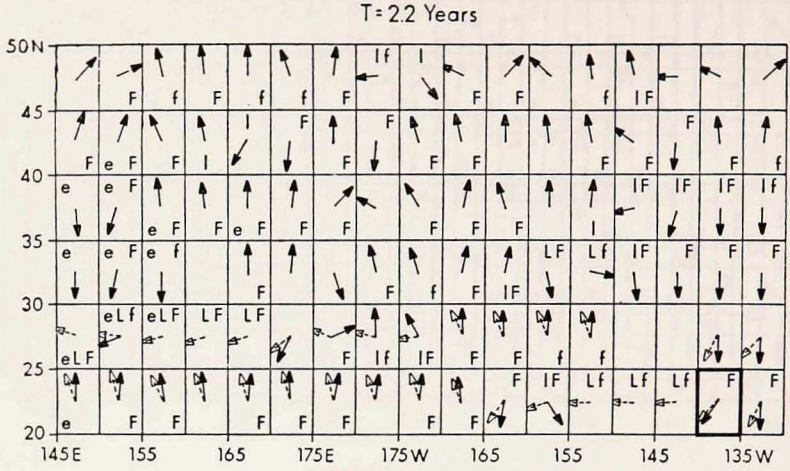

5. Results of the analysis

Figure 7 illustrates the direction of propagation of phase, γ, for each 5-degree square. The solid arrows represent the γ values found in the generalized model, while the open arrows represent the γ values found by constraining the model to Rossby wave dispersion (done for the zonal region 20-30N only). The absence of an arrow (solid, open, or both) indicates that either no best fit was found or the wave length of the best fit wave was larger than arbitrarily chosen 12,000 km. In addition, an "E" indicates that energy, E_1, was found to be greater than 10^{13} m^6s^{-3}, and an "*e*" is indicated wherever $10^{13} > E_1 \geq 10^{12}$ m^6s^{-3}. (The dimension of E_1 is obtained by squaring RBPE and dividing by angular frequency.) If the wave length, λ, was greater than 10^4 km an "*L*" is indicated, and for $10^4 > \lambda \geq 5 \times 10^3$ km, an "*l*" is indicated. "*F*" denotes cases where $50 \geq F_{min}/F_0 > 25\%$, and "*f*" shows where $25 \geq F_{min}/F_0 \geq 0\%$. (0% is a perfect fit; 100% means none of the RBPE fluctuations are accounted for by the model.) And finally, heavy lines around the perimeter of a square mean that the radius parameter, R_1, was within one standard deviation of the radius of the Rossby wave dispersion circle, i.e. cases where the generalized dispersion was only insignificantly different from Rossby wave dispersion.

For the 10-, 6.7-, and 5-year waves, squares marked by heavy lines yielded exactly Rossby wave dispersion. Strikingly, for the 10- and 6.7-year waves, these Rossby waves are the predominant feature in the 20-30N zone and account for slightly more than 50 percent (on the average) of the spectrally decomposed RBPE variance. At lower periods, however, Rossby waves did not result as best fit waves in many cases. Also, one can readily see that high-energy fluctuations are found in the west, predominantly between 25N and 40N, and that good fit cases are found all over the field. Table 1 summarizes the extent to which observed RBPE variance is accounted for by the generalized model.

Table 1. Percent of total number of squares where fit was good in the generalized model.

Wave Period	$0 \leqslant F_{min}/F_0 \leqslant 25\%$	$0 \leqslant F_{min}/F_0 \leqslant 50\%$
10	22	59
6.7	15	67
5	25	65
4	24	60
3.3	23	74
2.9	22	80
2.5	29	82
2.2	17	77

Closer examination reveals that high-energy fluctuations are also found in the 20-25N zone between 165W and 140W for the 10-, 6.7-, and 5-year cases and that these fluctuations exhibit Rossby dispersion and are good fit cases. The long wave length cases frequently occur with the high wave energy cases in the east. West of 180, long wave lengths are found predominantly between 25N and 40N with conspicuous occurrence in the 25-30N zone for wave periods of 10, 6.7, 5, 4, and 3.3 years.

The error bars for direction γ and wave length λ are quite large in some cases. As a sample, Table 2 lists best fit values (generalized model) of E_1, ϕ_1, λ, γ, and phase speed, C, and F_{min}/F_0 along with their standard deviations (prefixed by "δ") for the 10-year wave. Squares are identified by the longitude and latitude of their centers. (Asterisks in Table 2 mean that the number is too large to print; that number is infinite when R_1 and ϕ_1 error bars contain the wave number origin.)

Possible refraction phenomena are seen in several sequences of squares that manifest a smoothly varying trend in γ. For example, the 10-year waves in the region 25-30N, 170-140W show γ smoothly decreasing as energy propagates westward. There are, however, several cases throughout the field where adjacent squares exhibit large differences between their respective γ values. Refraction will be discussed further in the next section.

Finally, the question of the existence of Rossby waves at higher latitudes (above 30N) should be addressed. Kang and Magaard (1979) found two stable solutions to the equations of baroclinic instability of the North Pacific Current: the barotropic and first-order baroclinic Rossby shear modes. Figure 8 compares four of their numerically determined loci of wave number vectors (for two periods at two locations) with corresponding best fit wave numbers determined by our generalized model. (The "boxes" around each such point demark one standard deviation about its R_1 and ϕ_1 values.) The graphs reveal that these best fit points are consistently significantly different from the loci of those theoretical Rossby wave number vectors.

Table 2. Best fit wave parameters and their standard deviations found by the generalized model for the 10-year period.

T = 10.0 YEARS

Lat.	Lon.	E_1	δE_1	ϕ_1	$\delta\phi_1$	λ	$\delta\lambda$	γ	$\delta\gamma$	C	δC	F_{min}/F_0
(DEGREES)		$(M^6 S^{-3}) \times 10^{10}$		(DEGREES)		(KM)		(DEGREES)		(CM S^{-1})		%
47.5N	147.5E	208.	37.	-90.48	0.07	1600	300	-144.	12.	0.5	0.1	35.
47.5N	152.5E	107.	37.	-90.40	0.15	2100	1100	156.	148.	0.7	0.4	62.
47.5N	157.5E	112.	30.	-89.22	0.12	1200	200	0.	14.	0.4	0.1	51.
47.5N	162.5E	83.	21.	-89.35	0.11	1400	300	-6.	16.	0.4	0.1	54.
47.5N	167.5E	48.	13.	-89.35	0.11	1400	300	0.	17.	0.4	0.1	53.
47.5N	172.5E	32.	7.	-90.86	0.09	1100	100	174.	170.	0.3	0.0	48.
47.5N	177.5E	19.	3.	-90.62	0.07	1500	200	-174.	170.	0.5	0.1	44.
47.5N	177.5W	9.	1.	-90.31	0.06	2400	700	-144.	15.	0.8	0.2	27.
47.5N	172.5W	4.	1.	-90.20	0.11	4600	3700	-174.	122.	1.5	1.2	58.
47.5N	167.5W	1.	0.	-90.19	0.07	1000	100	102.	8.	0.3	0.0	52.
47.5N	162.5W	1.	0.	-90.24	0.10	2600	1800	132.	27.	0.8	0.6	57.
47.5N	157.5W	2.	0.	-90.17	0.08	3600	2600	-132.	28.	1.1	0.8	31.
47.5N	152.5W	2.	0.	-90.28	0.04	3200	600	162.	12.	1.0	0.2	14.
47.5N	147.5W	2.	1.	-90.10	0.10	5500	*****	126.	360.	1.7	*****	63.
47.5N	142.5W	4.	1.	-89.38	0.09	1500	300	-6.	14.	0.5	0.1	49.
47.5N	137.5W	7.	1.	-89.68	0.06	1500	300	60.	9.	0.5	0.1	71.
47.5N	132.5W	35.	10.	-89.94	0.12	3200	3200	78.	44.	1.0	1.0	66.
42.5N	147.5E	196.	24.	-90.52	0.05	1600	200	-180.	172.	0.5	0.1	18.
42.5N	152.5E	156.	33.	-90.24	0.08	2600	1300	138.	23.	0.8	0.4	36.
42.5N	157.5E	158.	24.	-90.00	0.06	18900	*****	-96.	360.	6.0	*****	23.
42.5N	162.5E	112.	18.	-89.90	0.06	6600	8700	-36.	43.	2.1	2.8	29.
42.5N	167.5E	68.	10.	-89.88	0.06	6600	4600	18.	45.	2.1	1.5	25.
42.5N	172.5E	43.	5.	-90.01	0.05	50300	*****	140.	360.	15.9	*****	25.
42.5N	177.5E	37.	5.	-90.43	0.05	2000	300	180.	170.	0.6	0.1	35.
42.5N	177.5W	27.	6.	-90.57	0.09	1500	300	-174.	166.	0.5	0.1	50.
42.5N	172.5W	11.	3.	-90.60	0.11	1400	300	180.	164.	0.4	0.1	56.
42.5N	167.5W	6.	2.	-90.54	0.13	1600	400	-180.	158.	0.5	0.1	61.
42.5N	162.5W	4.	1.	-90.06	0.12	11700	*****	-150.	360.	3.7	*****	67.
42.5N	157.5W	4.	1.	-90.49	0.09	1700	400	174.	164.	0.6	0.1	54.
42.5N	152.5W	4.	1.	-90.42	0.06	2000	300	168.	11.	0.6	0.1	21.
42.5N	147.5W	4.	1.	-90.54	0.11	1600	300	174.	163.	0.5	0.1	52.
42.5N	142.5W	8.	2.	-90.60	0.11	1400	300	180.	163.	0.4	0.1	65.
42.5N	137.5W	9.	2.	-89.17	0.10	1000	100	12.	10.	0.3	0.0	58.
42.5N	132.5W	8.	1.	-89.46	0.05	1600	200	-0.	8.	0.5	0.0	26.
37.5N	147.5E	1643.	430.	-90.25	0.09	3200	1500	-174.	143.	1.0	0.5	61.
37.5N	152.5E	1354.	508.	-90.43	0.14	1800	700	174.	151.	0.6	0.2	69.
37.5N	157.5E	830.	245.	-89.44	0.11	1400	300	-0.	16.	0.4	0.1	60.
37.5N	162.5E	757.	162.	-89.47	0.08	1500	200	6.	12.	0.5	0.1	61.
37.5N	167.5E	773.	262.	-89.49	0.12	1600	400	0.	21.	0.5	0.1	62.
37.5N	172.5E	326.	89.	-89.58	0.10	1800	500	-12.	20.	0.6	0.2	66.
37.5N	177.5E	116.	18.	-89.65	0.06	2200	400	-0.	13.	0.7	0.1	24.
37.5N	177.5W	65.	8.	-89.68	0.04	2400	400	-6.	11.	0.8	0.1	13.
37.5N	172.5W	19.	4.	-89.70	0.07	2600	700	0.	22.	0.8	0.2	37.
37.5N	167.5W	12.	2.	-89.68	0.05	2400	500	12.	13.	0.8	0.1	38.
37.5N	162.5W	14.	2.	-89.60	0.06	2000	300	6.	11.	0.6	0.1	44.
37.5N	157.5W	24.	6.	-90.30	0.09	2600	900	180.	154.	0.8	0.3	54.
37.5N	152.5W	26.	6.	-90.32	0.08	2400	700	180.	158.	0.8	0.2	47.
37.5N	147.5W	17.	3.	-90.37	0.06	2100	300	-174.	168.	0.7	0.1	20.
37.5N	142.5W	21.	2.	-90.43	0.03	1800	200	174.	6.	0.6	0.1	11.
37.5N	137.5W	21.	2.	-90.50	0.03	1600	100	-174.	4.	0.5	0.0	8.

37.5N	132.5W	15.	1.	-90.60	0.03	1300	100	-174.	4.	0.4	0.0	8.
32.5N	147.5E	1865.	413.	-89.98	0.08	19100	*****	59.	360.	6.1	*****	52.
32.5N	152.5E	2149.	401.	-89.99	0.06	51400	*****	-46.	360.	16.3	*****	34.
32.5N	157.5E	1602.	146.	-89.96	0.03	19100	55800	-17.	79.	6.1	17.7	11.
32.5N	162.5E	1297.	135.	-89.94	0.04	11700	10600	-12.	55.	3.7	3.4	20.
32.5N	167.5E	1175.	211.	-89.94	0.06	11700	*****	6.	88.	3.7	53.7	30.
32.5N	172.5E	470.	94.	-89.90	0.07	6600	9200	-24.	60.	2.1	2.9	43.
32.5N	177.5E	130.	15.	-89.82	0.04	4000	1000	-12.	16.	1.3	0.3	19.
32.5N	177.5W	63.	6.	-89.60	0.03	1800	200	6.	6.	0.6	0.1	20.
32.5N	172.5W	33.	6.	-89.45	0.06	1400	200	0.	8.	0.4	0.0	38.
32.5N	167.5W	33.	6.	-89.40	0.06	1200	100	-0.	7.	0.4	0.0	30.
32.5N	162.5W	57.	9.	-89.36	0.05	1100	100	6.	6.	0.4	0.0	26.
32.5N	157.5W	88.	11.	-89.31	0.04	1100	100	6.	4.	0.3	0.0	16.
32.5N	152.5W	87.	13.	-90.60	0.05	1200	100	-180.	174.	0.4	0.0	23.
32.5N	147.5W	76.	16.	-90.42	0.07	1700	300	174.	167.	0.6	0.1	43.
32.5N	142.5W	86.	22.	-90.26	0.09	2900	1100	-180.	150.	0.9	0.4	50.
32.5N	137.5W	49.	10.	-90.10	0.07	5500	10400	138.	39.	1.7	3.3	65.
32.5N	132.5W	16.	1.	-89.96	0.03	18900	42900	23.	73.	6.0	13.6	11.
27.5N	147.5E	322.	42.	-90.39	0.04	1700	200	-156.	8.	0.5	0.1	24.
27.5N	152.5E	435.	110.	-90.38	0.08	1800	500	171.	164.	0.6	0.1	58.
27.5N	157.5E	465.	160.	-90.09	0.11	6500	*****	149.	360.	2.0	*****	63.
27.5N	162.5E	301.	99.	-89.91	0.11	6700	*****	32.	360.	2.1	*****	65.
27.5N	167.5E	209.	63.	-89.74	0.10	2700	1300	12.	32.	0.8	0.4	59.
27.5N	172.5E	99.	26.	-89.75	0.08	2800	1200	13.	28.	0.9	0.4	62.
27.5N	177.5E	48.	12.	-90.04	0.08	10100	*****	127.	360.	3.2	*****	55.
27.5N	177.5W	35.	9.	-90.05	0.08	9400	*****	132.	360.	3.0	*****	52.
27.5N	172.5W	23.	6.	-90.08	0.09	6900	*****	147.	360.	2.2	*****	62.
27.5N	167.5W	23.	6.	-89.82	0.09	3800	2800	18.	42.	1.2	0.9	57.
27.5N	162.5W	46.	10.	-89.86	0.07	4700	3500	22.	38.	1.5	1.1	43.
27.5N	157.5W	69.	12.	-89.89	0.06	5900	5600	28.	38.	1.9	1.8	30.
27.5N	152.5W	75.	14.	-89.93	0.06	7900	46600	39.	74.	2.5	14.8	33.
27.5N	147.5W	78.	17.	-89.97	0.07	11100	*****	62.	360.	3.5	*****	42.
27.5N	142.5W	87.	22.	-89.97	0.08	11000	*****	60.	360.	3.5	*****	49.
27.5N	137.5W	46.	9.	-89.85	0.06	4400	2600	20.	32.	1.4	0.8	69.
27.5N	132.5W	16.	1.	-89.64	0.03	2000	200	9.	6.	0.6	0.1	16.
22.5N	147.5E											
22.5N	152.5E											
22.5N	157.5E	146.	45.	-90.42	0.10	1600	400	175.	163.	0.5	0.1	58.
22.5N	162.5E	77.	19.	-90.54	0.08	1300	200	176.	170.	0.4	0.1	59.
22.5N	167.5E											
22.5N	172.5E											
22.5N	177.5E	11.	1.	-90.51	0.04	1300	100	176.	175.	0.4	0.0	37.
22.5N	177.5W	6.	1.	-89.42	0.04	1200	100	4.	4.	0.4	0.0	27.
22.5N	172.5W	10.	2.	-89.56	0.07	1500	200	5.	10.	0.5	0.1	50.
22.5N	167.5W	25.	7.	-89.52	0.08	1400	300	5.	12.	0.4	0.1	53.
22.5N	162.5W	75.	19.	-89.47	0.08	1300	200	4.	10.	0.4	0.1	53.
22.5N	157.5W	151.	39.	-89.43	0.08	1200	200	4.	10.	0.4	0.1	48.
22.5N	152.5W	174.	47.	-89.40	0.08	1100	200	4.	10.	0.4	0.1	49.
22.5N	147.5W	142.	39.	-89.39	0.09	1100	200	4.	10.	0.4	0.1	50.
22.5N	142.5W	102.	25.	-89.38	0.08	1100	100	4.	8.	0.3	0.0	44.
22.5N	137.5W	64.	13.	-89.35	0.06	1000	100	3.	7.	0.3	0.0	37.
22.5N	132.5W											

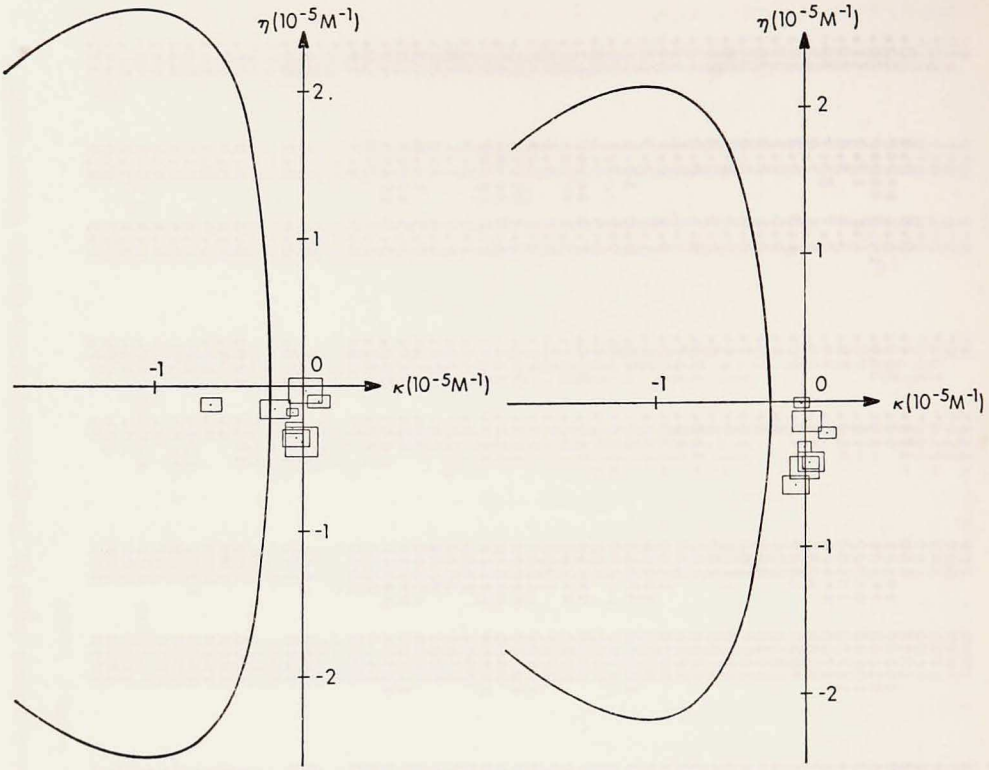

Figure 8. Comparison of best fit wave numbers (plotted with their one standard deviation error boxes) with the locus of the corresponding theoretical Rossby wave number vector for wave period 10 years in region 40-50N, 170-150W (a) and in region 40-50N, 170E-170W (b), and for wave period 6.7 years in region 40-50N, 170-150W (c) and in region 40-50N, 170E-170W (d). (Wave vector loci in (a) and (b) after Kang (unpublished) and in (c) and (d) after Kang and Magaard (1979).)

6. Discussion and conclusions

The persistence of 10- and 6.7-year Rossby waves as best fit waves in the generalized model applied to the 20-30N zone leads us to conclude that they are a dominant feature in this area. In the 40-50N zone, the best fit waves have significantly larger wave lengths than the theoretical Rossby wave modes calculated for this area by Kang and Magaard (1979). This suggests that Rossby waves at these periods do not play a major role in the higher latitudes. Nevertheless, more than 50 percent of the RBPE variance can be accounted for by the generalized model in 60-80 percent of all the squares (Table 1), with higher E_1 values found in the west where total RBPE variance is high. In addition, fluctuations in some areas have large length scales indicating that broad areas are fluctuating almost in phase.

The high-energy Rossby waves of 10-, 6.7-, and 5-year periods found in the

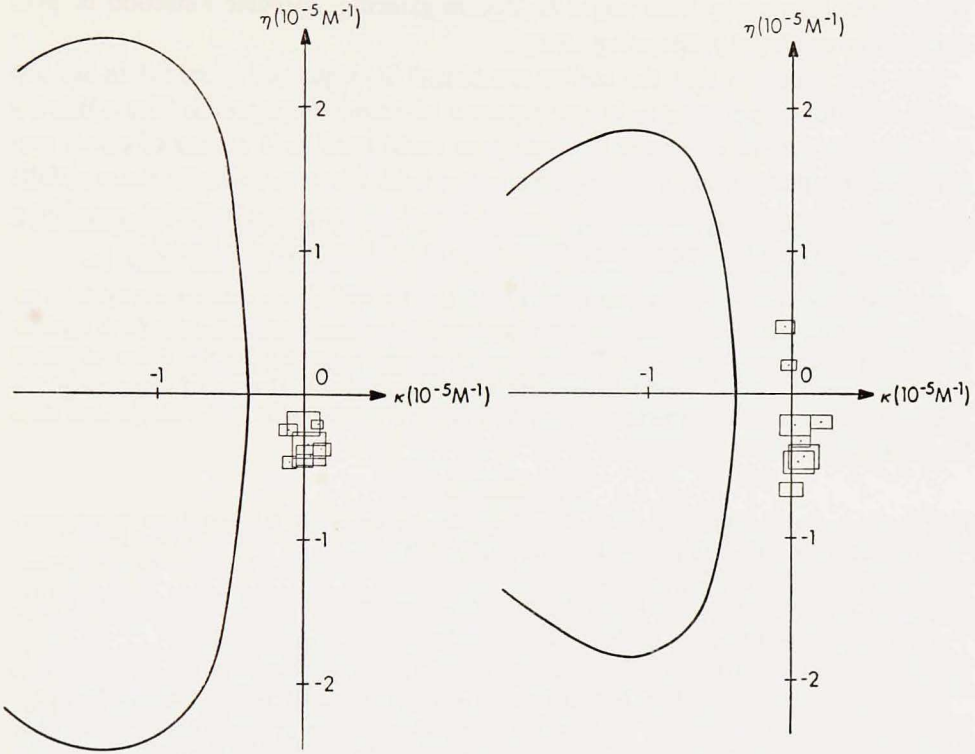

southeast corner of the field could be coastally generated waves with attenuating amplitude as energy propagates westward. Recent theoretical studies, White (1977b) and Schopf *et al.* (unpublished manuscript) predict an increase in meridional wave length as coastally generated Rossby wave energy propagates westward. Some sequences of our squares, e.g. 25-30N, 170-140W in the 10-year case, are in qualitative agreement with this prediction.

The distinct difference in phase propagation between the eastern and western halves of the 20-30N zone could be due to topography. The Hawaiian ridge (running approximately between 30N, 175E and 20N, 155W) seems to be the demarcation between the rapidly changing pattern in the west and the more regular pattern in the east. This is seen for all wave periods with a curious similarity between the 10- and 6.7-year cases. On the other hand, the less protrusive Emperor Seamount Chain (running approximately between 50N, 165E and 30N, 175E) does not appear to affect propagation of these waves. Generally rougher bottom topography west of 180 as well as possible wave-current interactions involving the Kuroshio could also be factors causing these refractions.

The pattern of phase propagation within the North Pacific Current contains some zonally adjacent squares, particularly in the 10- and 2.9-year cases, exhibiting nearly

180 degree differences. This might be due to glancing, specular reflection of predominantly westward propagating energy.

It is quite possible that the earlier mentioned inadequacies of our data set are responsible for some features in our patterns of phase propagation. The optimum interpolation used to overcome the data gaps could itself be a source of error, creating features that are not really present in the field. However, despite these pitfalls some persistent patterns emerge that might reveal (at least qualitatively) something about the mechanics of long wave propagation in the North Pacific basin.

Acknowledgments. We are grateful to Warren White for making his data set available to us. In addition, we thank Yong Kang for providing us with his unpublished Rossby wave number vector diagrams (Figs. 8a and 8b). This research has been supported by the Office of Naval Research under the North Pacific Experiment of the International Decade of Ocean Exploration; this support is gratefully acknowledged. The paper is Hawaii Institute of Geophysics Contribution No. 1046.

REFERENCES

Emery, W. J. and L. Magaard. 1976. Baroclinic Rossby waves as inferred from temperature fluctuations in the Eastern Pacific. J. Mar. Res., *34,* 365–385.

Kang, Y. Q. 1979. (unpublished results).

Kang, Y. Q. and L. Magaard. 1979. Stable and unstable Rossby waves in the North Pacific Current as inferred from the mean stratification. Dyn. Atmos. Oceans, *3,* 1–14.

Price, J. M. and G. Meyers. 1978. A climatology of potential density in the Central North Pacific, 20N-50N, 170E-150W. Hawaii Inst. of Geophys. Rep., HIG-78-4, Univ. of Hawaii.

Magaard, L. and J. M. Price. 1977. Note on the significance of a previous Rossby wave fit to internal temperature fluctuations in the Eastern Pacific. J. Mar. Res., *35,* 649–651.

White, W. B. 1977a. Secular variability in the baroclinic structure of the interior North Pacific from 1950-1970. J. Mar. Res., *35,* 587–607.

—— 1977b. Annual forcing of baroclinic long waves in the tropical North Pacific Ocean. J. Phys. Oceanogr., *7,* 50–61.

Schopf, P. S., D. L. T. Anderson, and R. Smith. Beta-dispersion of low frequency Rossby waves. Submitted to Dyn. Atmos. Oceans.

Received: *7 September, 1979;* revised: *25 February, 1980.*